Published OnlineFirst July 17, 2014; DOI: 10.1158/0008-5472.CAN-13-3334

Cancer Research

Osteopontin Shapes Immunosuppression in the Metastatic Niche

Sabina Sangaletti, Claudio Tripodo, Sara Sandri, et al.

Cancer Res 2014;74:4706-4719. Published OnlineFirst July 17, 2014.

Published OnlineFirst July 17, 2014; DOI: 10.1158/0008-5472.CAN-13-3334

Microenvironment and Immunology

Cancer Research

Osteopontin Shapes Immunosuppression in the Metastatic Niche

Sabina Sangaletti[1], Claudio Tripodo[2], Sara Sandri[1], Ilaria Torselli[1], Caterina Vitali[1], Chiara Ratti[1], Laura Botti[1], Alessia Burocchi[1], Rossana Porcasi[2], Andrea Tomirotti[1], Mario P. Colombo[1], and Claudia Chiodoni[1]

Abstract

The matricellular protein osteopontin (OPN, Spp-1) is widely associated with cancer aggressiveness when produced by tumor cells, but its impact is uncertain when produced by leukocytes in the context of the tumor stroma. In a broad study using *Spp1*$^{-/-}$ mice along with gene silencing in tumor cells, we obtained evidence of distinct and common activities of OPN when produced by tumor or host cells in a spontaneously metastatic model of breast cancer. Different cellular localization of OPN is associated with its distinct activities, being mainly secreted in tumor cells while intracellular in myeloid cells. OPN produced by tumor cells supported their survival in the blood stream, whereas both tumor- and host-derived OPN, particularly from myeloid cells, rendered the metastatic site more immunosuppressive. Myeloid-derived suppressor cells (MDSC) expanded with tumor progression at both primary and lung metastatic sites. Of the expanded monocytic and granulocytic cell populations of MDSCs, the monocytic subset was the predominant source of OPN. In *Spp1*$^{-/-}$ mice, the inhibition of lung metastases correlated with the expansion of granulocyte-oriented MDSCs. Notably, monocytic MDSCs in *Spp1*$^{-/-}$ mice were less suppressive than their wild-type counterparts due to lower expression of arginase-1, IL6, and phospho-Stat3. Moreover, fewer regulatory T cells accumulated at the metastatic site in *Spp1*$^{-/-}$ mice. Our data find correlation with lung metastases of human mammary carcinomas that are associated with myeloid cells expressing OPN. Overall, our results unveiled novel functions for OPN in shaping local immunosuppression in the lung metastatic niche. *Cancer Res; 74(17); 4706–19. ©2014 AACR.*

Introduction

Despite the advances in tumor prevention, early diagnosis, and therapeutic treatments, breast cancer remains one of the leading causes of death among women, mostly because of its predisposition to metastasize to distant sites, such as lungs, liver, brain, and bones. Much effort has been dedicated to the identification of molecular mechanisms conferring metastatic advantage to specific neoplastic clones so as to target the relevant pathways. Most of these pathways are also necessary for the local invasiveness of the primary tumor, and therefore their targeting may represent an appealing approach to contrast both aspects at the same time.

Besides genetically altered cancer cells, a tumor mass comprises a variety of normal cells that actively participate in tumor progression, including the metastatic process. Tumor and stromal cells produce the extracellular matrix (ECM), composed of structural proteins, such as collagens and fibronectin, and proteins that regulate cell function and their interaction, such as osteopontin (OPN, Spp-1), thrombospondin, SPARC (secreted protein acidic and rich in cysteine), and others, collectively referred to as matricellular proteins. These molecules are generally highly expressed during development, poorly in steady-state condition of adult tissues, whereas readily upregulated in wound healing and tissue remodeling. Matricellular proteins modulate several cellular processes, such as cell adhesion and migration, ECM deposition, cell survival, and proliferation (1). All these processes are also required for primary tumor growth and metastasis, in which matricellular proteins are often aberrantly expressed.

Among matricellular proteins, elevated OPN expression has been correlated with poor survival of patients with cancer with different tumor histotypes (2–4). Accordingly, clinical studies have shown high OPN plasma concentration in patients with metastatic tumors compared with normal samples, especially in breast cancer (5, 6). OPN protumoral and prometastatic activities have been demonstrated in mice and humans (1, 7, 8)

[1]Molecular Immunology Unit, Department of Experimental Oncology and Molecular Medicine, Fondazione IRCCS Istituto Nazionale Tumori, Milan, Italy. [2]Tumor Immunology Unit, Human Pathology Section, Department of Health Sciences, University of Palermo, Palermo, Italy.

Note: Supplementary data for this article are available at Cancer Research Online (http://cancerres.aacrjournals.org/).

M.P. Colombo and C. Chiodoni share senior authorship for this article.

Current address for S. Sandri: Immunology Section, Department of Pathology and Diagnostics, University of Verona, Verona, Italy.

Corresponding Authors: Mario P. Colombo, Molecular Immunology Unit, Department of Experimental Oncology and Molecular Medicine, Fondazione IRCCS Istituto Nazionale Tumori, Via Amadeo 42, 20133, Milan, Italy. Phone: 39-02-2390-2252, ext. 2212; Fax: 39-02-2390-3073; E-mail: mariopaolo.colombo@istitutotumori.mi.it; and Claudia Chiodoni, claudia.chiodoni@istitutotumori.mi.it

doi: 10.1158/0008-5472.CAN-13-3334

Published OnlineFirst July 17, 2014; DOI: 10.1158/0008-5472.CAN-13-3334

through the modulation of tumor cell migration, adhesion, and invasion (9–12).

Nevertheless, the comprehension of molecular mechanisms behind OPN functions in cancer remains far from complete (13). Most studies were centered on OPN produced by tumor cells, whereas only few have focused on OPN produced by the host (14–16), moreover without considering the metastatic setting.

This study, designed to dissect the role of OPN produced by either the tumor or the host in the context of breast cancer, provided the first evidence of OPN tuning the immunosuppressive microenvironment of the metastatic niche.

Materials and Methods

Cell line and mice

The 4T1 cell line (CRL-2539; LGC-Promochem) was derived from a murine spontaneous mammary carcinoma arising in a BALB/cfC3H mouse (17). BJMC3879 is a mammary adenocarcinoma developed in a BALB/c female upon inoculation into the inguinal mammary glands of mouse mammary tumor virus (MMTV; refs. 18, 19) and was kindly provided by Dr. Shibata (Osaka Medical College, Osaka, Japan). Female BALB/c mice, 8-week-olds, were purchased from Charles River Laboratories. C57BL/6 *spp1*$^{-/-}$ mice (B6.129S6(Cg)-Spp1^{tm1Blh}/J) were obtained from The Jackson Laboratory and backcrossed on BALB/c background for 10 generations. Mice were maintained at the Fondazione IRCCS Istituto Nazionale Tumori (Milan, Italy) under standard conditions according to the institutional guidelines. All *in vivo* procedures were approved by the Institute Ethical Committee for animal use.

OPN gene silencing

Stable OPN gene silencing was obtained with the BLOCK-iT Pol II miR RNAi Expression Vector Kit from Invitrogen (see Supplementary Data for details and silencing sequences); Western blot analysis and ELISA on cell supernatants confirmed protein downmodulation (see Supplementary Data), whereas immunohistochemistry was performed on paraffin-embedded sections of primary tumor samples to confirm *in vivo* downmodulation.

In vitro migration, soft-agar colonization, anoikis, and adhesion assays

The motility of the 4T1 parental and silenced cells was evaluated in Transwell chambers as previously described (for more details, see Supplementary Data; ref. 20).

Anchorage-independent growth was determined in 0.3% agarose (SeaPlaque; FMC BioProducts) with a 0.6% agarose underlay. Cells (3×10^3) were plated in semisolid medium (DMEM 10% FBS plus agar 0.3%) and incubated at 37°C in a humidified 5% CO_2 atmosphere. Colonies were counted under a microscope, blindly by two operators, after 8 to 12 days.

For an *in vitro* anoikis assay, 5×10^5 cells were plated into 6-well tissue-treated plates previously coated or not with polyhydroxyethylmethacrylate (poly-HEMA; Sigma-Aldrich), in DMEM supplemented with 10% FBS or 2% FBS. After 20-hour incubation at 37°C, cells were collected, and anoikis was assessed counting viable cells:dead cells ratio by Trypan blue staining, blindly by two operators.

An adhesion assay was performed in 6-well plates in which 1G11 endothelial cells (a kind gift of Dr. Vecchi, Humanitas, Milan, Italy) were previously seeded 48 hours before (24 + 24 hours in the presence or absence of TNF, at 5 ng/mL to induce cell activation). 4T1GFP and 4T1silOPN GFP cells (5×10^4) were added and let to adhere for 30 minutes; after PBS1x wash, cells were collected by trypsinization and GFP$^+$ cells were evaluated by flow cytometry.

In vivo experiments

Parental, silenced, or control cell lines were inoculated orthotopically in the mammary fat pad (i.f.p.) at a dose of 5×10^4 cells per mouse or intravenously (i.v.) at a dose of 10^4 cells per mouse. For BJMC3879, 5×10^6 cells per mouse were used. Primary tumor growth was measured once a week with a caliper, and the volume was calculated using the formula $d^2 \times D/2$, where d and D are the short and long diameters, respectively.

For micrometastasis evaluation, lungs were removed from each mouse 28 days after tumor injection, and a clonogenic assay was performed (see Supplementary Data). For macrometastasis evaluation, lungs were removed after intratracheal perfusion with 15% China ink and fixed with Fekete solution (10% formaldehyde; 5% acetic acid in Et-OH 70%). Metastases, identified as white spots, were counted blindly by two operators. Alternatively, metastases were counted on H&E (hematoxylin and eosin)-stained lung sessions under the microscope.

For a lung colonization assay, 4T1 cells or 4T1 silOPN527, both expressing GFP, were injected i.v. (2×10^6 cells/mouse) in BALB/c mice. Peripheral blood leukocytes (PBL) were drawn at 2, 4, 8, 16, 24, and 48 hours and analyzed by flow cytometry for the presence of GFP$^+$ CD45.2$^-$ cells. For lung evalution, 1, 3, 4, and 5 days after cells injection, mice were sacrificed, their lungs minced, digested with collagenase/hyaluronidase solution (STEMCELL Technologies), and analyzed by flow cytometry.

Histopathologic and immunohistochemical analysis

Samples, fixed in 10% neutral buffered formalin, were embedded in paraffin. Serial sections were cut at 4 μm from each block and stained with H&E. For immunohistochemical staining, the sections were dewaxed and rehydrated. After heat-mediated antigenic retrieval using a pH 9.0 Tris–EDTA buffer for 30 minutes in thermostatic water bath, the sections were incubated with 3% hydrogen peroxide for 5 minutes to quench endogenous peroxidase activity, and for 10 minutes with protein block (Novocastra, Ltd.). The sections were subsequently incubated with primary antibodies: anti-human/mouse OPN (dilution, 1:100; R&D Systems, Inc.), anti-P-Stat3 (dilution, 1:200; Acris Antibodies, GmbH), and anti-human CD68 (dilution, 1:100; Dako). For negative controls, mouse or rabbit immune sera were used instead of primary antibodies. Staining was revealed with a polymeric system (Novolink, Max Polymer Detection System; Novocastra Ltd.) and visualized by using AEC$^+$ High Sensitivity Substrate Chromogen Ready-to-

Published OnlineFirst July 17, 2014; DOI: 10.1158/0008-5472.CAN-13-3334

use (Dako Cytomation Liquid AEC Substrate Chromogen System; Dako). Slides were counterstained with hematoxylin and evaluated under a Leica DM2000 optical microscope.

Double-marker immunofluorescence and confocal microscopy

For double immunofluorescence, two sequential rounds of single-marker immunofluorescence were performed using CD68/OPN and CD68/arginase-1 markers. The sections were incubated with the first primary antibody (OPN or arginase-1) overnight at 4°C in a humidified chamber, then washed in PBS, and incubated for 1 hour with an Alexa Fluor 488–conjugated anti-rabbit antibody (dilution, 1:100) for arginase-1 and with an Alexa Fluor 488–conjugated anti-goat secondary antibody (dilution, 1:100) for OPN. Then, the slides were washed in PBS and incubated with CD68 for 1 hour, which was revealed using an Alexa Fluor 568–conjugated anti-mouse Ab (dilution 1:200). The sections were counterstained with DAPI (DNA stain) for 1 minute and mounted using coverslip with a drop of mounting medium.

For confocal microscopy analysis, myeloid cells or 4T1 cells were seeded onto poly-D-lysine–coated glasses, let to adhere, and 2 hours later, fixed with PFA 4%. For intracellular staining of OPN, glasses were sequentially incubated with 0.1% Triton X-100, 1% BSA, polyclonal rabbit anti-OPN (Abcam), in 0.1% BSA solution and Alexa Fluor 546 anti-rabbit secondary antibody. For staining of the endoplasmic reticulum (ER) concanavalin A (Alexa Fluor 488–conjugated; Life Technologies) was added as the final step. Glasses were analyzed with a Microradiance 2000 (Bio-Rad Laboratories) confocal microscope equipped with Ar (488 nm), HeNe (543 nm), and red laser diode (638 nm) lasers. Confocal images (512 × 512 pixels) were obtained using a 20×, 0.5 NA Plan Fluor DIC or 60×, 1.4 NA oil immersion lens and analyzed using ImagePro 7.0.1 software.

FACS analysis

For FACS analysis, primary tumors or lungs were collected and perfused with DMEM plus 10% FBS, minced, and then filtered through a 40-μm-pore cell strainer (BD Biosciences). Red blood cells were removed using ACK lysis buffer (ammonium chloride potassium). Cells were Fc-blocked using CD16/32 antibody (eBioscience) before staining. The following antibodies were used: CD45.2, Gr-1, CD11b, F4/80, Ly6C, CD11c, CD4 and CD8, CD44, CD69, and CD62L (all from eBioscience). For regulatory T cells (Treg) detection, after surface staining for CD4, cells were fixed, permeabilized, and stained with FoxP3 Ab, following the manufacturer's instructions (eBioscience).

Samples were acquired using a BD LSR II Fortessa instrument and analyzed with FlowJo software (TreeStar). All samples are analyzed in single; in each experiment, at least three to four samples were analyzed for each group.

Myeloid-derived suppressor cell purification and *in vitro* suppression assay

Myeloid-derived suppressor cells (MDSC) were purified using CD11b-conjugated microbeads (for overall population) and the Myeloid-Derived Suppressor Cell Isolation Kit (for separation of the two subsets; Miltenyi Biotec) following the manufacturer's instructions.

For an *in vitro* suppression assay, 4×10^5 naïve BALB/c splenocytes were labeled with carboxyfluorescein succinimidyl ester (CFSE; Sigma-Aldrich) and cocultured with the different MDSC population at different ratios in the presence of 2 μg/mL of soluble anti-CD3 and 1 μg/mL of anti-CD28 to activate lymphocytes. Each sample was seeded in triplicate. Proliferation of CD4 and CD8 T cells was assessed 2 and 3 days later, by flow cytometry evaluating CFSE dilution in the $CD4^+$- and $CD8^+$-gated populations. Results are shown as the percentage of proliferated cells.

RNA extraction and qPCR

For qPCR analysis, MDSC subsets and other leukocyte populations were purified from the lungs of tumor-bearing mice, pooling at least 5 mice per group; lungs were minced and digested for 45 minutes at 37°C in collagenase/hyaluronidase solution, washed with complete medium, and stained with the specific Abs before cell sorting with a FACSAria instrument (BD Biosciences). Purity of the different population was >99%.

RNA was purified from TRIzol (Invitrogen)-disrupted cells by phenol/chloroform extraction followed by loading onto an RNeasy MINI or MICRO kit (Qiagen). On-column DNAse treatment was routinely performed. RNA purity and yield was assessed using NanoDrop. RNA was reverse transcribed using the High-Capacity cDNA Reverse Transcription Kit (Applied Biosystems). qPCR reaction was prepared using TaqMan Fast Universal PCR Master Mix and run on a 7900 HT Fast Real-time PCR System (Applied Biosystems). The following TaqMan probes were used: *Gapdh* (Mm99999915_g1), *Spp1* (Mm00436767_m1), *Arg-1* (Mm00475988_m1), *Nos2* (Mm00440502_m1), *Il6* (Mm00446190_m1), *Stat3* (Mm01219775_m1), *Vegf* (Mm01281449_m1), and (Mm01178820_m1).

Statistical analysis

For evaluation of lung metastases, data were represented singularly, and median was shown in the graph; statistical significance was evaluated with the Mann–Whitney test using Prism 5 software. For all the other experiments, data were represented as mean ± SD, and an unpaired two-tailed Student *t* test was used for statistical analysis.

Results

RNA interference of OPN expression affects *in vitro* and *in vivo* metastatic phenotype of mammary adenocarcinoma

RNA interference was used to generate stable OPN-silenced 4T1 mammary cancer cells using three different sequences, 215, 527, and 602 (see Materials and Methods and Supplementary Data). Efficiency of gene silencing was evaluated by Western blot analysis on cell lysates and by ELISA on cell supernatants (Supplementary Fig. S1A and S1B); as a control we used cells transduced with nontarget sequence (4T1 NT). Initial *in vitro* and *in vivo* experiments were conducted with all the three silenced clones, and with clone 527 thereafter (4T1silOPN527).

Published OnlineFirst July 17, 2014; DOI: 10.1158/0008-5472.CAN-13-3334

Migratory ability of silenced clones assessed across Transwell membranes was significantly inhibited in comparison with that of parental and NT control (Supplementary Fig. S1C). Consistently, OPN neutralization by an anti-OPN antibody markedly diminished the migration of 4T1 wild-type (WT) and control cells (Supplementary Fig. S1D). Anchorage-independent growth, evaluated in soft agar, showed no difference in the number of colonies (Supplementary Fig. S1E, top), despite a reduction in size of 4T1silOPN527 colonies (bottom). No difference was detected in proliferation rate *in vitro* (not shown).

OPN-silenced 4T1 cells and their WT and NT control counterparts injected into the mammary fat pad formed primary tumors with similar size and onset (Fig. 1A). Immunohistochemical analysis of OPN expression on tumor nodules

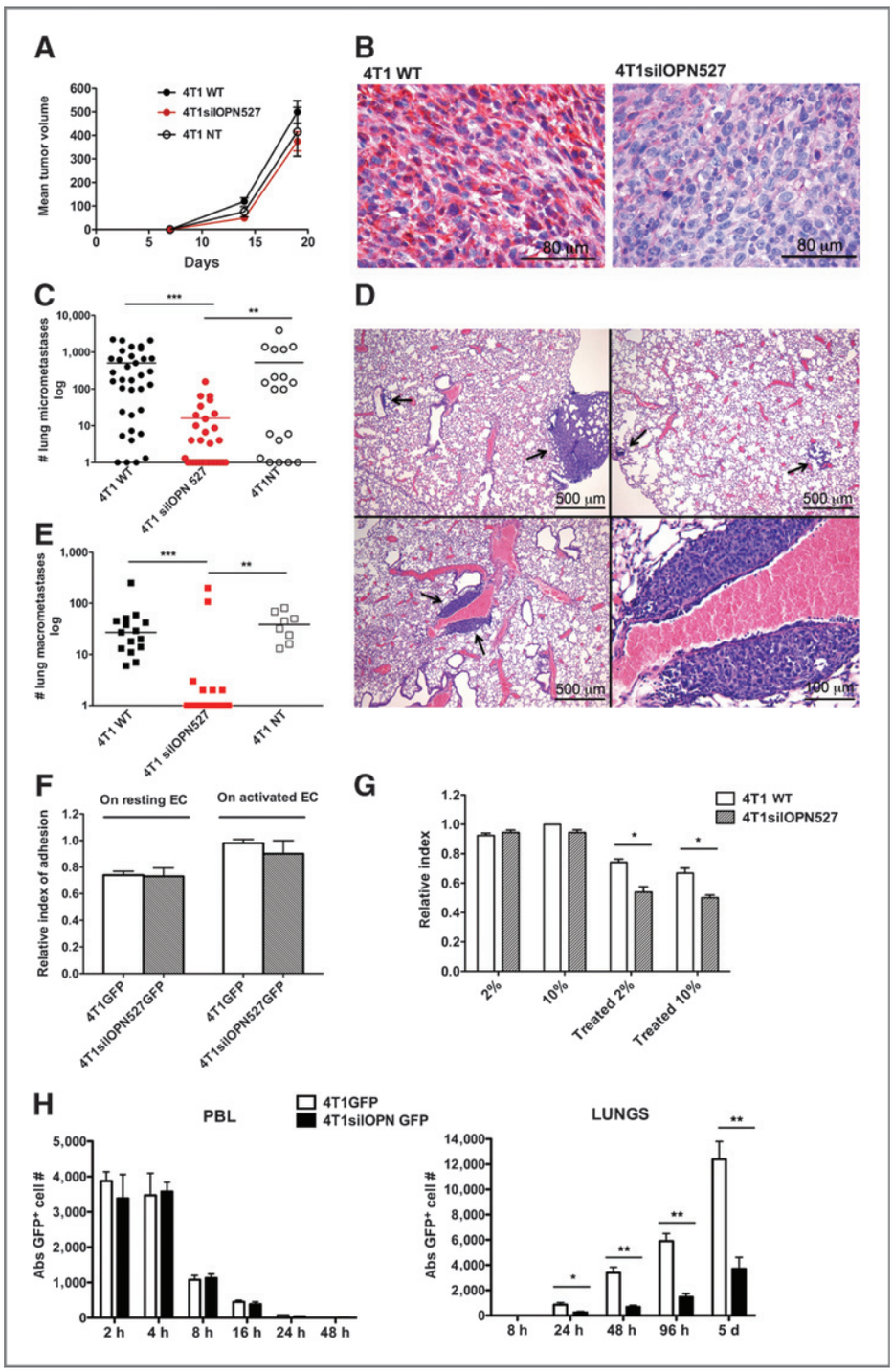

Figure 1. OPN silencing in tumor cells reduces their metastatic potential, affecting survival in lung circulation and lung colonization. A, primary tumor growth of OPN-silenced 4T1 cells in comparison with parental and NT cells. Tumor volume is measured by caliper and calculated as $(d^2 \times D)/2$. The graph is a pool of four different experiments, each performed with 7 mice per group. B, OPN staining in primary tumor samples from 4T1 parental and OPN-silenced cells. C, spontaneous lung micrometastases after orthotopic injection i.f.p., evaluated by a clonogenic assay, of 4T1 cells OPN-silenced, WT, and control NT. A pool of four experiments is shown; 5–7 mice per group for each experiment. D, representative images of lungs from 4T1-bearing mice, either WT or OPN-silenced. E, experimental lung macrometastases upon i.v. injection, counted after ink perfusion, of 4T1 cells OPN-silenced, WT, and control NT. A pool of two experiments is shown; 5–7 mice per group for each experiment (repeated at least three times). F, *in vitro* adhesion experiment of 4T1GFP and 4T1silOPNGFP tumor cells on endothelial cells (1G11) either resting or upon 24 hours TNF activation. Cells were plated in triplicate; experiment performed twice. G, anoikis *in vitro* assay of 4T1 cells OPN-silenced and WT control; cells were seeded in triplicates onto poly-HEMA–treated plates in the presence of 2% or 10% FBS; experiment was performed twice. H, PBL (left) and lung parenchyma (right) colonization at early time points after i.v. injection of 2×10^6 4T1GFP and 4T1silOPNGFP tumor cells. Lung tissue was digested, and cell suspension from lungs and PBL analyzed by FACS for GFP^+ cells; cells were gated on the $CD45.2^-$ population; experiment was performed three times, with three samples per group for each time point. *, $P < 0.05$; **, $P < 0.01$; ***, $P < 0.005$.

Published OnlineFirst July 17, 2014; DOI: 10.1158/0008-5472.CAN-13-3334

confirmed efficient OPN downmodulation in the case of silencing (Fig. 1B). On the other hand, the evaluation of spontaneous metastases showed that OPN-silenced 4T1 clones have significantly reduced metastatic capacity (Fig. 1C and D and Supplementary Fig. S1F).

Injection of tumor cells directly into the blood stream bypasses the initial steps of the metastatic process such as tumor detachment and cell intravasation. Intravenous injection of 4T1silOPN527 cells induced significantly less metastases to the lungs than OPN-proficient controls, indicating that tumor-derived OPN is required for a late step of metastasis, from circulation to the seeding into the target organ (Fig. 1E). Consistently, other OPN-silenced clones were also less metastatic upon i.v. injection (Supplementary Fig. S1G).

Tumor cell–produced OPN was not required for adherence to resting or activated endothelial cells as tested *in vitro* (Fig. 1F). However, the ability to survive in the bloodstream was different, in agreement with the known activity of OPN-protecting cancer cells from apoptosis (21): 4T1silOPN527 cells showed increased cell death than parental 4T1 cells when cultured in nonadherent condition *in vitro* (Fig. 1G) and at early time points after *in vivo* i.v. inoculation. Indeed, when we i.v. injected GFP-expressing 4T1 cells and evaluated their numbers in PBL and lungs at early time points after injection, we found that GFP^+ 4T1silOPN527 cells were fewer in number than GFP^+ parental 4T1 cells in the lungs starting 24 hours after injection and thereafter. We excluded an uneven number of cells injected because the amount of GFP^+ cells, either OPN-proficient or -deficient, in PBL was similar at earlier time points (2, 4, 8, and 16 hours; Fig. 1H).

Host-derived OPN contributes to the metastatic spread of breast cancer polarizing myeloid cells toward immunosuppression

Once demonstrated that tumor-derived OPN works mainly autocrinally, conferring survival advantage in anoikis conditions, we tested whether or not host-produced OPN contributed to metastasis. This possibility stems from the reported activity of OPN in skewing macrophages to a M1 phenotype through downmodulation of IL10 and upregulation of IL12 production (22), and could, theoretically, negatively affect tumor growth and metastasis. Therefore, we injected 4T1 cells in WT and $Spp1^{-/-}$ mice and, to exclude any masking effect exerted by the high endogenous expression of OPN by 4T1 parental cells, 4T1silOPN527 cells were also included.

4T1 cells formed significantly lower numbers of metastases in $Spp1^{-/-}$ mice than WT counterparts (Fig. 2A), despite similar primary tumor growth (not shown), demonstrating that host-derived OPN also contributes to metastasis. The lower metastatic ability of 4T1 cells in $Spp1^{-/-}$ mice was confirmed in the case of i.v. injection, indicating that host-derived OPN is required at later stages of metastasis directly at the seeding organ (Fig. 2B). The paucity of 4T1silOPN527 metastasis in WT mice did not allow us to detect further decrease in metastasis in $Spp1^{-/-}$ animals (Fig. 2A).

Whether accessory cells involved in breast cancer metastasis, such as macrophages (23), MDSC (24–26), and T cells (27, 28), might use OPN to favor the metastatic process remains unknown.

First, we analyzed the MDSC population, identified as $CD11b^+/Gr\text{-}1^+$ cells in the mouse, because of their reported role in 4T1 breast cancer metastasis (25, 29, 30) and of their huge expansion in the lungs of tumor-bearing mice, where they represent 70% to 80% of the infiltrating leukocytes. Overall, the number of $CD11b^+/Gr\text{-}1^+$ cells was not different in lungs of $Spp1^{-/-}$ and WT tumor-bearing mice, whereas splitting the myeloid population into the two subsets of $Gr\text{-}1^{high}$ (granulocytic) and $Gr\text{-}1^{int/low}$ (monocytic) cells highlighted a significant change in their ratio: expanded $Gr\text{-}1^{high}$ subset in $Spp1^{-/-}$ mice at the expense of the $Gr\text{-}1^{int/low}$, more suppressive, one (Fig. 2C). Such difference was tumor induced because lungs and spleens of tumor-free mice showed a similar ratio between the two subsets regardless of the *Spp1* genotype (Supplementary Fig. S2A). As OPN may have a role in protection from apoptosis, we determined whether lung MDSC from $Spp1^{-/-}$ tumor bearers had a different apoptotic rate than their WT counterparts. AnnexinV/PI flow cytometry did not show strain difference for either subset (data not shown).

Notably, the $Gr\text{-}1^{int/low}$ subset expressed *Spp1* at a much higher level than the $Gr\text{-}1^{high}$ population, as tested by qPCR and confirmed by double immunofluorescence, showing OPN expression mainly in $CD68^+$ cells with monocytic appearance (Fig. 2D). This result raised the question of whether OPN plays a role in MDSC immunosuppression.

An *in vitro* suppressive assay, performed using the purified $Gr\text{-}1^{high}$ and $Gr\text{-}1^{int/low}$ subsets, showed that $Gr\text{-}1^{int/low}$ cells from WT mice were significantly more suppressive than their $Spp1^{-/-}$ counterparts against CD3/CD28-activated CD8 and CD4 T cells (Fig. 3A and Supplementary Fig. S2B). As expected, the suppressive ability of $Gr\text{-}1^{int/low}$ cells was higher than that of the $Gr\text{-}1^{high}$ subset.

To better characterize the $Gr1^{high}$ and $Gr\text{-}1^{int/low}$ subsets from metastatic lungs of $Spp1^{-/-}$ and WT mice, qPCR was performed on genes relevant for MDSC function. Arginase-1 (*Arg-1*), *Tgfb1*, *Il6*, and *Stat3* were higher in the $Gr\text{-}1^{int/low}$ than in the $Gr1^{high}$ subsets; vice versa, *Nos2* was higher in the $Gr1^{high}$ than in the $Gr\text{-}1^{int/low}$ cells (Fig. 3B). Strikingly, *Arg-1* expression in the $Gr\text{-}1^{int/low}$ subset was repressed in $Spp1^{-/-}$ mice, supporting the idea of a less suppressive phenotype we observed in the absence of OPN (Fig. 3A). A similar trend, although not statistically significant, was observed for *Stat3*, *Il6*, *Tgfb1*, and *Vegf*, with their expression reduced in $Spp1^{-/-}$ mice. In metastatic lungs, double immunofluorescence analysis confirmed the colocalization of OPN and arginase-1 (Fig. 3C), whereas IHC for phospho (P)-STAT3 stained only cells with a monocytic appearance, which was represented more in WT than $Spp1^{-/-}$ mice (Supplementary Fig. S3).

To test whether OPN from MDSC was truly relevant for the metastatic spread of 4T1 cells, coinjection experiments were performed. WT, but not $Spp1^{-/-}$, MDSC isolated from the spleen of tumor-bearing mice increased lung metastases when coinjected with 4T1 cells (Fig. 3D), and even more significantly when coinjected into $Spp1^{-/-}$ hosts. No effect was observed when bone marrow–derived macrophages

Published OnlineFirst July 17, 2014; DOI: 10.1158/0008-5472.CAN-13-3334

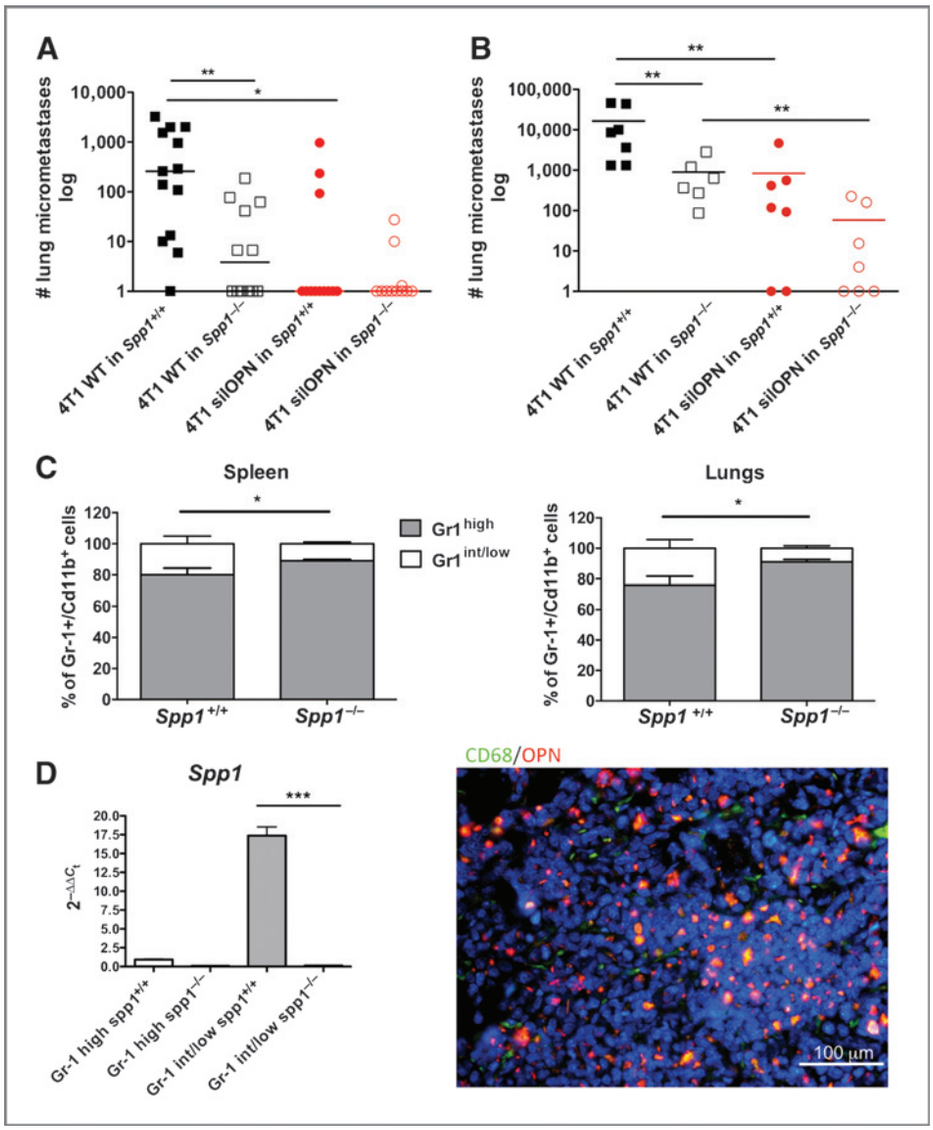

Figure 2. Host-derived OPN contributes to lung metastasis, affecting MDSC polarization. A, spontaneous lung micrometastases, evaluated by the clonogenic assay, of WT and OPN-silenced 4T1 cells in WT and Spp1$^{-/-}$ mice after orthotopic injection i.f.p. A pool of two experiments is shown and experiment was repeated four times for 4T1 WT with 6 to 7 mice per group and twice for OPN-silenced cells. B, experimental lung micrometastases of WT and OPN-silenced 4T1 cells in WT and Spp1$^{-/-}$ mice after i.v. injection. One representative experiment out of three was performed; 6 to 7 mice per group. C, MDSC polarization in lungs and spleen of 4T1 tumor-bearing mice, either WT or Spp1$^{-/-}$. Mean and SD of 5 mice per group is shown. The experiment was repeated four times. D, expression of OPN assayed by qPCR in the MDSC subsets (Gr1^{high} and Gr1$^{int/low}$) from lungs of WT and Spp1$^{-/-}$ tumor-bearing mice (left). The WT Gr-1^{high} MDSC subset was used as a reference (=1). Mean of three samples per group; each sample is a pool of 4 to 5 mice; experiment was repeated three times. Right, immunofluorescence for OPN (red) and for the monocytic marker CD68 (green) in the lungs of WT mice. *, $P < 0.05$; **, $P < 0.01$; ***, $P < 0.005$.

from either *Spp1*$^{-/-}$ or WT mice were partners of the coinjection (not shown).

These results indicate that myeloid cell–produced OPN favors the metastatic spread of 4T1 carcinoma.

Host-derived OPN molds immunosuppression at the metastatic site

To test whether host OPN deficiency affected other leukocyte populations infiltrating the lungs of tumor-bearing mice, we performed multiparametric FACS analysis comparing *Spp1*$^{-/-}$ and WT mice. No substantial difference in total CD11b^{+} cells (confirming the previous data) and overall CD4^{+} T cells and CD8^{+} T cells was detected. Nevertheless, intracellular staining for the FoxP3 transcription factor, identifying regulatory T cells (Treg), showed a reduced frequency of CD4^{+}FoxP3^{+} cells in *Spp1*$^{-/-}$ mice (Fig. 4A), a result confirmed by IHC analysis on lung sections (Fig. 4B). A reduced Treg number was associated with increased frequency of CD4^{+}-activated T cells (detected as CD44^{+}CD69^{+} and CD62L^{low}CD69^{+} cells) in *Spp1*$^{-/-}$ mice (Supplementary Fig. S4A and S4B). On the same leukocyte populations, sorted from the lungs of tumor-bearing mice, we evaluated by qPCR the level of *Spp1* expression to assess whether other cells, besides MDSC, express it. We confirmed a high *Spp1* level in the Gr-1$^{int/low}$ MDSC subset, whereas other leukocytes express it at a much lower level (Supplementary Fig. S4C).

Altogether, these data point to a role of host-derived OPN, mostly from monocytic MDSC, in tuning the immunosuppressive microenvironment of the metastatic lung niche.

Tumor-produced OPN contributes to local immunosuppression

We tested whether tumor-produced OPN contributed to molding the local immunosuppression in lung metastases. No significant differences were observed in leukocytes distribution and ratio in 4T1silOPN527 versus 4T1 metastatic lungs;

Published OnlineFirst July 17, 2014; DOI: 10.1158/0008-5472.CAN-13-3334

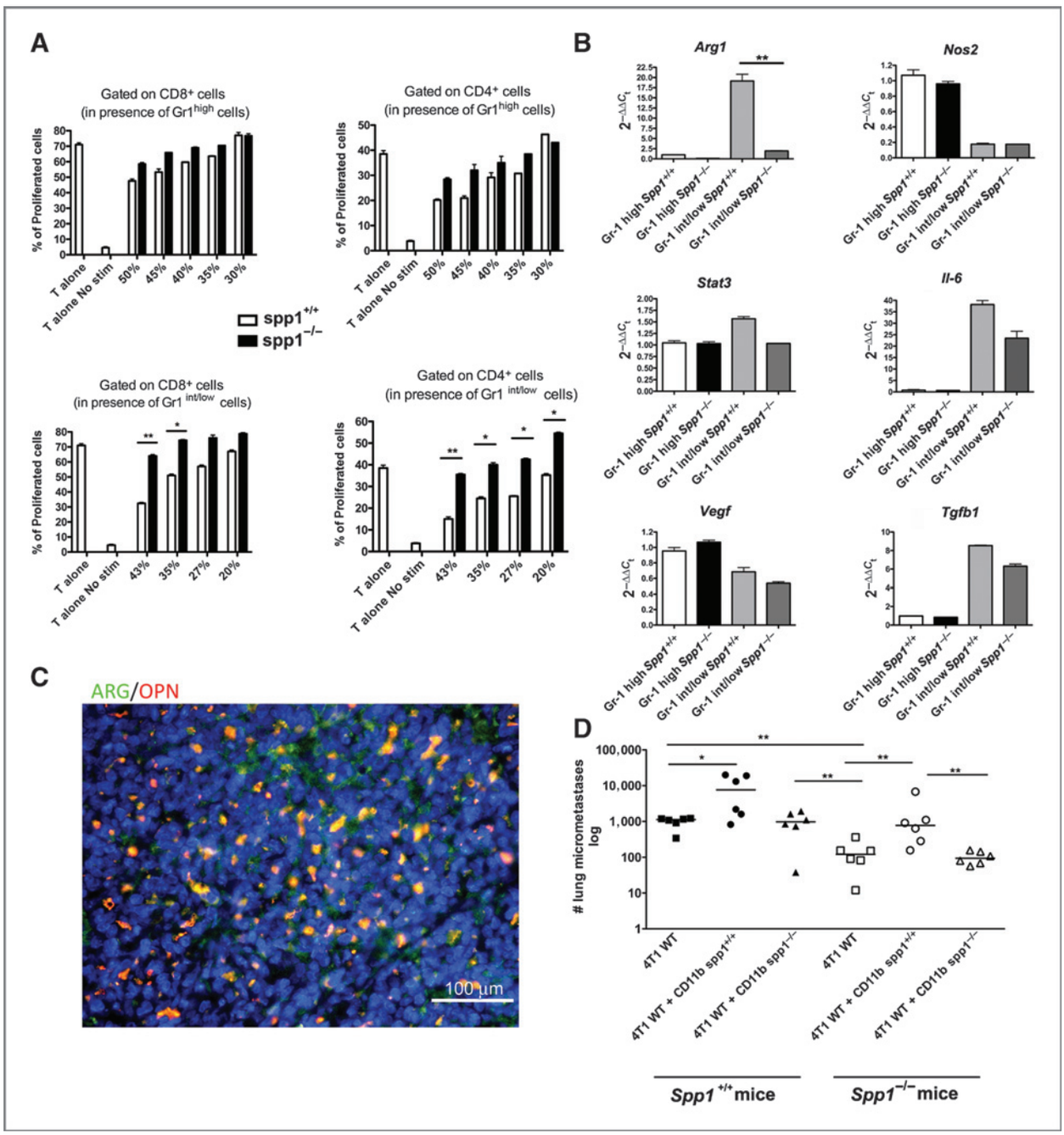

Figure 3. OPN molds the suppressive phenotype of MDSC, contributing to the metastatic potential of 4T1 cells. A, *in vitro* immunosuppressive activity of the two subsets of MDSC from the lungs of WT and Spp1$^{-/-}$ tumor-bearing mice on CD4 and CD8 T-cell proliferation; the suppressive activity was evaluated 3 days later. Samples are in triplicates. The experiment was performed three times, with overlapping results. B, expression of Arg-1, Nos2, Stat3, Il6, Vegf, and Tgfb1 in the MDSC Gr1^{high} and Gr1$^{int/low}$ subsets by qPCR; the WT Gr-1^{high} MDSC subset was used as a reference (=1). Samples are in duplicates; each one is a pool of 4 to 5 mice; one experiment is shown, out of the two performed. C, immunofluorescence showing colocalization of arginase-1 (green) and OPN (red) expression in myeloid cells in lungs of WT tumor-bearing mice. D, *in vivo* coinjection experiment of tumor cells with CD11bþ cells purified from tumor-bearing mice (either WT or Spp1$^{-/-}$) into WT and Spp1$^{-/-}$ mice. Cell mix (1:1) was injected i.f.p. Experiment was repeated twice.

MDSC number and ratio, as well as Treg number, were similar in lungs of mice bearing either parental or OPN-silenced 4T1 tumors (not shown). However, the analysis of *in vitro* suppressive activity of MDSC isolated from the lungs of mice bearing 4T1 cells or their OPN-silenced counterpart showed less suppression of T-cell proliferation in case Gr1$^{int/low}$ cells were from mice bearing 4T1silOPN527 tumors (Fig. 5A). Accordingly, this subset expressed lower level of *Arg1* and *Nos2* than its

Published OnlineFirst July 17, 2014; DOI: 10.1158/0008-5472.CAN-13-3334

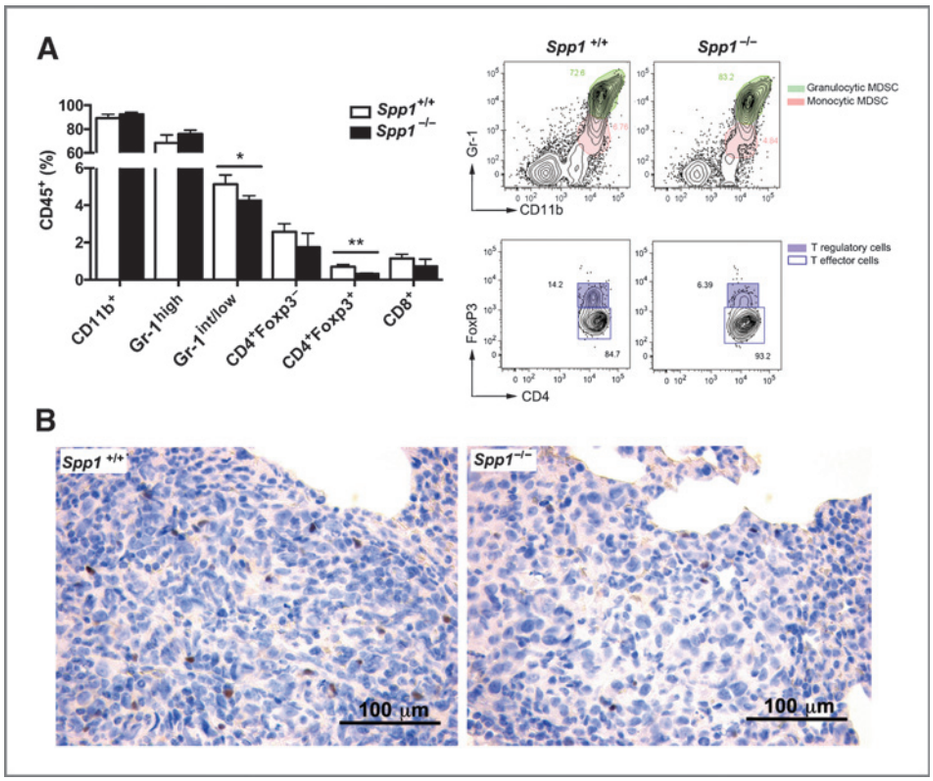

Figure 4. The absence of OPN influences the number of Treg in lungs of tumor-bearing mice. A, left, leukocyte infiltration in the lungs of WT or Spp1$^{-/-}$ tumor-bearing mice by multiparametric FACS analysis with the following markers: CD45.2, CD11b, Gr-1, CD4, CD8 (surface), and FoxP3 (intracellular). Cells are shown as percentage of CD45^{+} cells. Graph shows the mean of four samples for each group; experiment was performed four times. Right, examples of FACS plot for the MDSC subsets (Gr-1^{high} and Gr1$^{int/low}$) and Treg (FoxP3^{+} cells, gating on CD4^{+} cells) from the lungs of WT and Spp1$^{-/-}$ tumor-bearing mice. *, $P < 0.05$; **, $P < 0.01$. B, IHC of FoxP3^{+} Treg in lungs of WT and Spp1$^{-/-}$ mice bearing 4T1 tumors.

counterpart isolated from 4T1 WT tumor-bearing mice (Fig. 5B). No different expression for *Il6*, *Vegf*, *Tgfb1*, and *Stat3* was detected (not shown).

Considering that 4T1silOPN cells produce less metastases than the 4T1 counterpart, their contribution in terms of immunomodulatory factors should be reduced, explaining the lower immunosuppressive capacity of myeloid cells infiltrating these metastatic lungs. Either alternatively or concomitantly, the downmodulation of OPN expression in tumor cells may alter their secretion of immunosuppressive factors. This was indeed the case, at least for *Vegf* and *Il6* that were less expressed in OPN-silenced tumor cells (Fig. 5C).

Different form and cellular localization of OPN may account for the various activities of tumor- and host-derived OPN

Although tumor-derived OPN contributes to shaping MDSC immunosuppressive activity, 4T1 cells, fully competent for OPN production, are not able to compensate for the absence of OPN in the host, and when injected into *Spp1*$^{-/-}$ mice, these cells show severely impaired metastatic ability.

To explain such observation, we considered the recently described intracellular form of OPN (iOPN), which has been found enriched in cells of the monocytic lineage (31), and we hypothesized that tumor cells produce OPN mainly in the secreted form (sOPN), whereas myeloid cells in the intracellular form.

We evaluated the amount of sOPN in the supernatant from tumor and myeloid cells in relation to their OPN expression by qPCR. One million 4T1 tumor cells secreted roughly 1 μg/mL/24 hours of OPN, which was almost undetectable in the supernatant from myeloid cells (Fig. 6A). Although gene expression data by qPCR confirmed the trend of a much higher level in tumor cells than in myeloid cells, the ratio is not so striking as in the ELISA assay (300× vs. 10,000× in qPCR and ELISA, respectively; Fig. 6B). In addition, considering that qPCR data account for both sOPN and iOPN, it is likely that most OPN from tumor cells is secreted, whereas that from myeloid cells is retained in the cell. This interpretation was confirmed by confocal analysis showing that in tumor cells OPN was mainly cytoplasmic and colocalized with concanavalin A (staining ER), whereas in monocytic myeloid cells, OPN remained confined to specific spots under the cellular membrane, as reported in ref. 31, and not localized in the ER (Fig. 6C).

The requirement for host-produced OPN in lung metastasis is not restricted to the 4T1 tumor model

To assess whether host-derived OPN favors metastatic dissemination of mammary carcinomas other than the 4T1 model, the BJMC3879 adenocarcinoma (18, 19), another spontaneously metastasizing BALB/c breast tumor, was tested. Along with tumor progression, BJMC3879 expanded CD11b^{+}/Gr-1^{+} cells in PBL, spleen, and lungs (data not shown) and, phenocopying 4T1 cells, produced similar primary tumors but less lung metastases in *Spp1*$^{-/-}$ than WT mice (Fig. 7A–C). In addition, similar to the 4T1 model, the CD11b^{+}/Gr-1^{+} cell population showed an increase in the Gr-1^{high} fraction in the absence of OPN (Fig. 7D). These data indicate that the effect of

Published OnlineFirst July 17, 2014; DOI: 10.1158/0008-5472.CAN-13-3334

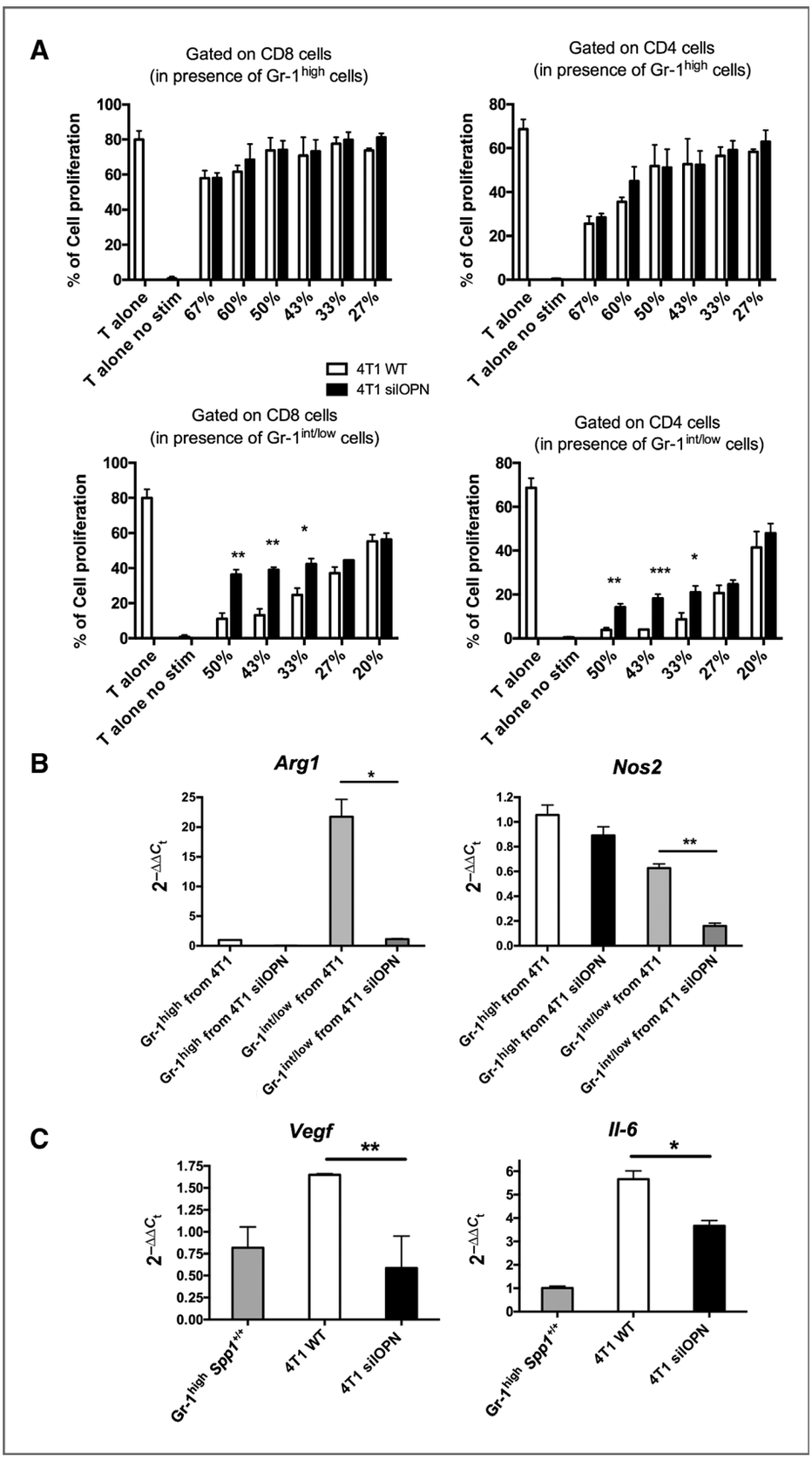

Figure 5. Role of tumor-derived OPN in the modulation of MDSC activity. A, *in vitro* suppressive activity of the Gr-1^{high} and Gr-1$^{int/low}$ subsets isolated from the lungs of mice bearing 4T1 WT and 4T1silOPN tumors. Naïve T cells were stained with CFSE and then seeded with scalar doses of Gr-1^{high} or Gr-1$^{int/low}$ cells in the presence of α-CD3 and α-CD8 Abs for stimulation. Suppressive activity was evaluated 3 days later. Each sample is in triplicate. Graphs show mean and SD of the triplicates. B, real-time PCR for Arg1 and Nos2 in the Gr-1^{high} and Gr-1$^{int/low}$ subsets isolated from the lungs of mice bearing 4T1 WT and 4T1silOPN tumors. Each sample is a pool of 7 mice; qPCR was performed twice on the same samples. Gr-1^{high} cells from 4T1 WT–bearing mice were used as a reference (=1). C, real-time PCR for Vegf and IL-6 in 4T1 and 4T1silOPN cells in comparison to Gr-1^{high} cells from 4T1WT–bearing mice was used as a reference. The experiment was performed in triplicate and repeated twice (*, $P < 0.05$; **, $P < 0.01$).

Published OnlineFirst July 17, 2014; DOI: 10.1158/0008-5472.CAN-13-3334

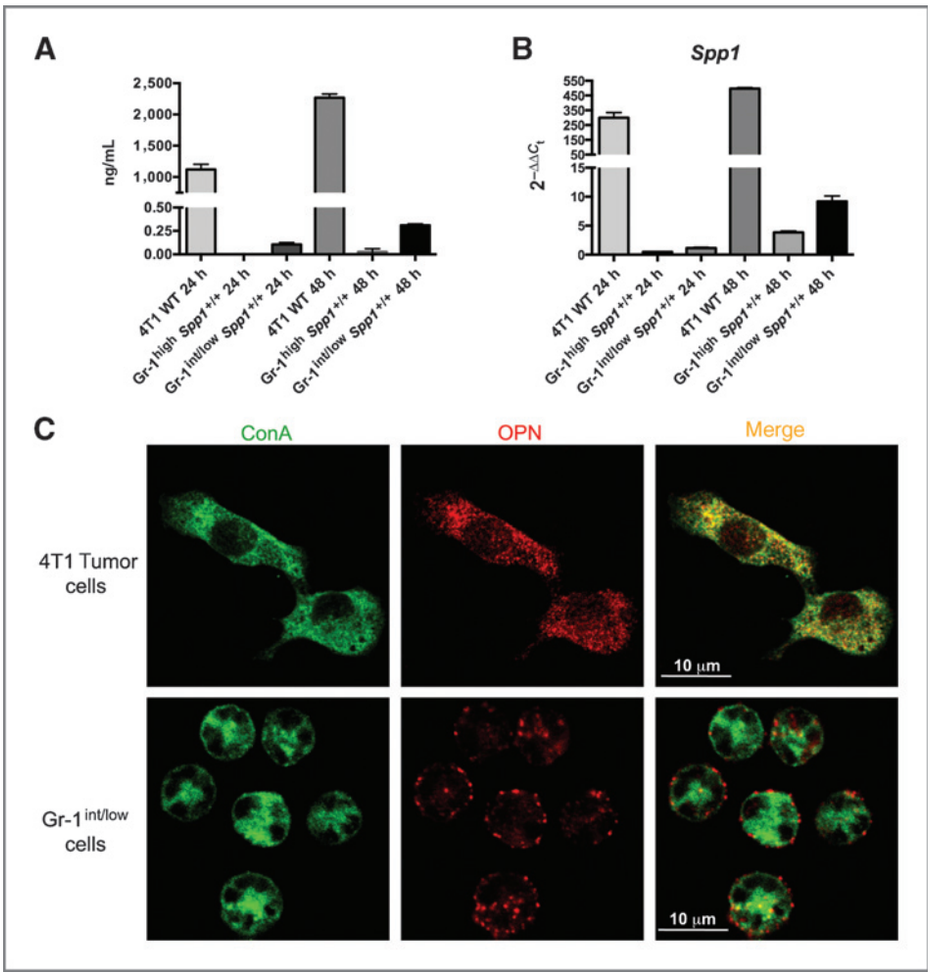

Figure 6. Tumor and myeloid cells show different cellular localization of OPN. A, quantification of OPN in the supernatants of 4T1 tumor cells and of the MDSC subsets by ELISA. Cells were seeded in 6- or 24-well plates at 10^6 cells/mL, in complete medium, and supernatants recovered at 24 and 48 hours. The ELISA Kit (R&D Systems) was performed following the manufacturer's instructions. Experiment was performed twice on different supernatant samples. B, real-time PCR for Spp1 expression on the same samples, recovering the cells in TRIzol and extracting RNA as described in Materials and Methods. The WT Gr-$1^{int/low}$ MDSC subset at 24 hours was used as a reference (=1). C, confocal analysis of OPN localization in tumor and myeloid cells. OPN (red) and concanavalin A (green) for Golgi and ER staining. Single and merged channels are shown.

host-produced OPN in breast cancer lung metastasis is not restricted to the 4T1 tumor model.

OPN stains myeloid cells in lung metastasis from breast cancer patients

To assess whether our finding in the mouse models has any clinical correlation, we evaluated the expression of OPN in lung metastases from 5 patients with breast cancer undergoing metastasectomy (see Supplementary Table S1 for clinical parameters). In the cases evaluated, OPN expression was detected in cells with monocytic morphology infiltrating metastatic cancer foci (Fig. 7E). Double immunofluorescence analysis using Abs for human OPN and the monocytic/macrophagic marker CD68 confirmed the myeloid/monocytic nature of OPN-expressing cells infiltrating breast carcinoma lung metastases (Fig. 7F).

Discussion

Tumor development and progression require a suitable microenvironment in which tumor cells conscript and corrupt normal resident cells, such as fibroblasts and endothelial cells, while recruiting accessory cells from the bone marrow toward their needs (32). Besides cellular elements, tumor stroma comprises the ECM, a complex network of macromolecules with different physical, biochemical, and biomechanical properties, also relevant for tumor progression and metastasis (33). Among matricellular proteins, OPN has been extensively studied as a tumor cell product conferring migratory, adhesive, and growth capacity. Whether OPN produced by stromal cells contributes to tumor progression and metastasis has not been defined. Here, we have dissected the role of OPN in breast cancer primary tumor growth and metastasis when its production was either tumor or host derived. Whereas our data substantially agree with the available literature in finding tumor-derived OPN prometastatic, the effect on primary tumor was negligible in our models, while rather relevant in other transplantable tumors (34–37). The effects of OPN inhibition in tumor cells have been investigated mainly *in vitro* testing cell adhesion, migration, invasion through Matrigel (34, 35, 37) or cell proliferation (38). Silencing OPN in 4T1 tumor cells, we obtained concordant inhibition of cell migration and invasion but no effect in cell proliferation and adhesion to different substrates (data not shown). Such *in vitro* effects, however, found little correlation with the *in vivo* metastatic activity we observed, in which tumor-produced OPN renders

Published OnlineFirst July 17, 2014; DOI: 10.1158/0008-5472.CAN-13-3334

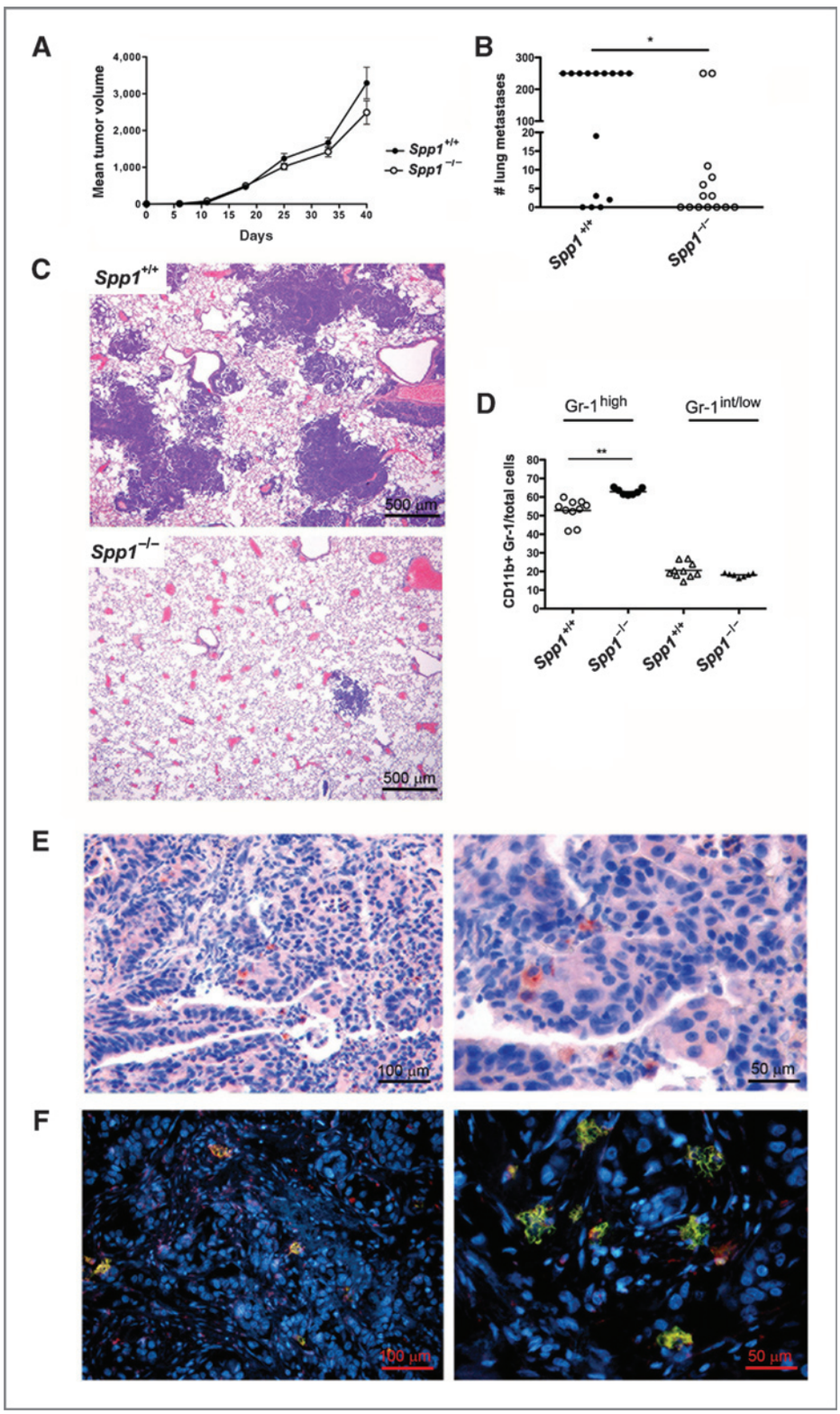

Figure 7. Host-derived OPN effect on metastasis is not model restricted. A, primary tumor growth of BJMC3879 mammary tumor cell line (5×10^6 cells i.f.p.) in WT and Spp1$^{-/-}$ mice. Tumor volume is measured by caliper and calculated as $(d^2 \times D)/2$. The graph is a pool of two different experiments; each performed with 7 mice per group. B, lung metastases after i.f.p. injection of BJMC3879 cells in WT and Spp1$^{-/-}$ mice; mice were sacrificed at day 40 to 45 after tumor injection and lung metastases were evaluated by H&E staining on serial lung sessions, blindly by two different operators. The graph is a pool of two experiments; each performed with 7 mice per group. C, representative images of lungs from WT and Spp1$^{-/-}$ mice injected i.f.p. with BJMC3879 cells. H&E staining. D, the Gr-1^{high} and Gr-1$^{int/low}$ subsets in WT and Spp1$^{-/-}$ mice bearing BJMC3879 mammary tumors. Graph, representative of one experiment out of two performed. E, immunohistochemical analysis of OPN expression on lung sessions from patients with breast cancer (see Supplementary Table S1 for clinical parameters) with lung dissemination. OPN stains large cells with monocytic appearance. F, double immunofluorescence on lung sessions from patients with metastatic breast cancer for OPN (green) and monocytic marker CD68 (red). DAPI, blue channel.

the cells intrinsically more resistant to apoptosis while in the blood stream, rather than favoring detachment from the primary site or intravasation. Accordingly, we found a similar antimetastatic effect of OPN silencing, using both intra-mammary fat pad and intravenous injection routes and did not observe any difference in the epithelial-to-mesenchymal

Published OnlineFirst July 17, 2014; DOI: 10.1158/0008-5472.CAN-13-3334

transition (EMT) phenotype between OPN-silenced or WT primary tumors (not shown). Nevertheless, data showing smaller soft-agar colonies (Fig. 1D), and smaller metastatic foci in the lungs of mice injected with OPN-silenced tumor cells, suggest that OPN might also contribute to lung parenchyma colonization.

Here, we provide novel findings showing that host-derived OPN, in particular from myeloid cells, molds the immunosuppressive microenvironment at the metastatic niche. The metastatic potential of mammary tumors was greatly reduced when the recipient mice were OPN deficient, despite the fact that tumor was fully competent for OPN production, and the primary tumor grew unmodified. The analysis of the immune microenvironment at the metastatic site (i.e., lungs) showed that OPN favors the presence of immunosuppressive leukocytes, and that such leukocytes were less suppressive in *Spp1*$^{-/-}$ mice. Myeloid cells endowed with suppressive activity, generally termed MDSC, comprise two main subsets in the mouse, which can be distinguished by the different expression of the Gr-1 marker: highly expressed on the most abundant, and poorly suppressive, granulocytic subpopulation (Gr-1^{high}), whereas expressed at low to intermediate level in the highly suppressive monocytic subset (Gr-1$^{int/low}$). Such MDSC are massively recruited to both primary tumor and metastatic lungs in the 4T1 mammary carcinoma (39, 40). We show here that in *Spp1*$^{-/-}$ mice, the ratio of the two subsets is significantly different, with a less abundant Gr-1$^{int/low}$-suppressive population (Fig. 2C). Interestingly, OPN expression seems to be mainly confined to the monocytic subset, suggesting that OPN may directly contribute to their immunosuppressive phenotype. Indeed, when tested for their ability to suppress T-cell proliferation *in vitro*, Gr-1$^{int/low}$ cells from lungs of 4T1-bearing *Spp1*$^{-/-}$ mice were less suppressive than their WT counterparts (Fig. 3A). We hypothesize that the different ratio of the two MDSC subsets in favor of the Gr1^{high} population and the reduced suppressive activity of the remaining Gr-1$^{int/low}$ subset create a lung microenvironment less permissive to metastasis. The reduced suppression of *spp1*$^{-/-}$ Gr-1$^{int/low}$ cells correlated with a lower expression of *Arg-1*, *IL6*, and *Stat3*, all marks of immunosuppression highly expressed in OPN-proficient MDSC (Fig. 3B). *In vivo*, coinjection of tumor cells with MDSC from either *Spp1*$^{-/-}$ or WT mice confirmed that only those from WT mice promoted metastasis of 4T1 cells, regardless of the *Spp1* genotype of recipient mice (Fig. 3D). Whether MDSC are produced or recruited differently from the bone marrow or whether they can transdifferentiate locally in relation to *Spp1* genotype is currently unknown.

The absence of host OPN seems to affect other aspects of local immune response in the lung metastatic niche, that is, it associates with a decrease in the number of Treg and with enhanced activation of CD4 T cells. Although OPN influences MDSC-suppressive activity, it does not modify Treg–mediated immunosuppression, at least *in vitro*, according to our unpublished data. Whether the effect on Treg number depends directly on the different MDSC population in *Spp1*$^{-/-}$ versus WT mice deserves further investigation.

The MDSC compartment was affected not only by host-derived but also by tumor-produced OPN (Fig. 5), likely because OPN-silenced tumors form less metastases and contribute less in producing immunosuppressive factors, such as VEGF and IL6.

Despite such contribution from tumor-derived OPN, 4T1 cells, fully competent for OPN production, are not able to compensate their absence in the host, and when injected into *Spp1*$^{-/-}$ mice show severely impaired metastatic ability. To explain this datum, we investigated OPN localization in tumor and myeloid cells. Indeed, other than the soluble OPN, an intracellular form (iOPN) has been recently identified in leukocytes, particularly in cells of the monocytic lineage (31). Combining dosage of secreted OPN by ELISA with qPCR expression analysis and confocal microscopy (Fig. 6), we demonstrate that tumor cells produce OPN in high amount in the secreted form, localized within the Golgi apparatus and ER. Differently, in myeloid cells, OPN is mainly condensed in specific spots localized in perimembrane areas, phenocopying the described iOPN localization (33).

The newly described role of host-derived OPN in metastasis was corroborated using a different spontaneously metastatic breast carcinoma model, the BJMC3879 cell line (41), that formed less spontaneous lung metastases when injected into *Spp1*$^{-/-}$ mice (Fig. 7A–D). Very few reports analyzed the role of host-produced OPN in tumor progression (14, 15, 35). Two reports (14, 15) studied carcinogen-induced papilloma and cutaneous squamous cell carcinoma (SCC), induced directly into *Spp1*$^{-/-}$ mice, therefore in complete absence of OPN in both host and tumors. The study from Chakraborty and colleagues (35) was the only one on breast cancer and showed a protumorigenic activity of host-derived OPN through the induction of oncogenic molecules, such as MMPs and uPA, and of angiogenesis, without considering the effect on metastasis.

Our demonstration that myeloid-derived OPN contributes to the immunosuppressive environment required for metastasis opens the question of whether other matricellular proteins may regulate tumor-associated immune responses and adds a whole new pathway to those involved in MDSC fitness. Moreover, this study further enforces the concept that matricellular proteins may produce different effects at discrete phases of tumor progression, according to their tumor-intrinsic or microenvironment-associated expression (42).

Notably, our data find clinical correlation in the presence of myeloid cells producing OPN in lung metastases of human ductal mammary carcinomas. In these samples, OPN expression was detected in scattered reactive cells with monocytoid morphology that were mostly localized within the stroma at the interface between the metastatic foci and the surrounding lung parenchyma, suggesting a role in the local events underlying constitution of the metastatic niche. The in-depth characterization of OPN-expressing cancer-associated myeloid populations and their potential biologic/prognostic relevance in cancer patient cohorts will represent an appealing issue of investigation.

In conclusion, our work is the first to show a role for both tumor- and host-derived OPN toward metastatic dissemination

Published OnlineFirst July 17, 2014; DOI: 10.1158/0008-5472.CAN-13-3334

through the modulation of local immunosuppression in the lung metastatic niche.

Disclosure of Potential Conflicts of Interest

No potential conflicts of interest were disclosed.

Authors' Contributions

Conception and design: M.P. Colombo, C. Chiodoni
Development of methodology: S. Sandri, C. Chiodoni
Acquisition of data (provided animals, acquired and managed patients, provided facilities, etc.): S. Sangaletti, C. Tripodo, S. Sandri, I. Torselli, C. Vitali, C. Ratti, L. Botti, A. Burocchi, A. Tomirotti
Analysis and interpretation of data (e.g., statistical analysis, biostatistics, computational analysis): S. Sangaletti, C. Tripodo, S. Sandri, C. Vitali, C. Chiodoni
Writing, review, and/or revision of the manuscript: S. Sangaletti, C. Tripodo, M.P. Colombo, C. Chiodoni
Administrative, technical, or material support (i.e., reporting or organizing data, constructing databases): R. Porcasi
Study supervision: M.P. Colombo, C. Chiodoni

Acknowledgments

The authors thank Dr. Shibata (Osaka, Japan) for providing the BJMC3879 cell line and Ivano Arioli and Barbara Cappetti for technical assistance. The authors also thank the Conventional and Confocal Microscopy Facility for confocal acquisition, and the Cell Sorting Facility for MDSC subsets cell sorting of the institute.

Grant Support

This work was supported by the Associazione Italiana per la Ricerca sul Cancro (AIRC: Investigator Grants 10137 to M.P. Colombo and Program Innovative Tools for Cancer Risk Assessment and Diagnosis, 5 per mille n°12162 to M.P. Colombo and C. Tripodo; MFAG n° 12810 to S. Sangaletti) and the Italian Ministry of Health.

The costs of publication of this article were defrayed in part by the payment of page charges. This article must therefore be hereby marked *advertisement* in accordance with 18 U.S.C. Section 1734 solely to indicate this fact.

Received November 25, 2013; revised May 29, 2014; accepted June 13, 2014; published OnlineFirst July 17, 2014.

References

1. Chiodoni C, Colombo MP, Sangaletti S. Matricellular proteins: from homeostasis to inflammation, cancer, and metastasis. Cancer Metastasis Rev 2010;29:295–307.
2. Furger KA, Menon RK, Tuck AB, Bramwell VH, Chambers AF. The functional and clinical roles of osteopontin in cancer and metastasis. Curr Mol Med 2001;1:621–32.
3. Rudland PS, Platt-Higgins A, El-Tanani M, De Silva Rudland S, Barraclough R, Winstanley JH, et al. Prognostic significance of the metastasis-associated protein osteopontin in human breast cancer. Cancer Res 2002;62:3417–27.
4. Patani N, Jouhra F, Jiang W, Mokbel K. Osteopontin expression profiles predict pathological and clinical outcome in breast cancer. Anticancer Res 2008;28:4105–10.
5. Singhal H, Bautista DS, Tonkin KS, O'Malley FP, Tuck AB, Chambers AF, et al. Elevated plasma osteopontin in metastatic breast cancer associated with increased tumor burden and decreased survival. Clin Cancer Res 1997;3:605–11.
6. Bramwell VH, Doig GS, Tuck AB, Wilson SM, Tonkin KS, Tomiak A, et al. Serial plasma osteopontin levels have prognostic value in metastatic breast cancer. Clin Cancer Res 2006;12:3337–43.
7. Rittling SR, Chambers AF. Role of osteopontin in tumour progression. Br J Cancer 2004;90:1877–81.
8. El-Tanani MK. Role of osteopontin in cellular signaling and metastatic phenotype. Front Biosci 2008;13:4276–84.
9. Wai PY, Mi Z, Guo H, Sarraf-Yazdi S, Gao C, Wei J, et al. Osteopontin silencing by small interfering RNA suppresses *in vitro* and *in vivo* CT26 murine colon adenocarcinoma metastasis. Carcinogenesis 2005;26:741–51.
10. Jessen KA, Liu SY, Tepper CG, Karrim J, McGoldrick ET, Rosner A, et al. Molecular analysis of metastasis in a polyomavirus middle T mouse model: the role of osteopontin. Breast Cancer Res 2004;6:R157–69.
11. Mi Z, Guo H, Russell MB, Liu Y, Sullenger BA, Kuo PC. RNA aptamer blockade of osteopontin inhibits growth and metastasis of MDA-MB231 breast cancer cells. Mol Ther 2009;17:153–61.
12. Sun BS, Dong QZ, Ye QH, Sun HJ, Jia HL, Zhu XQ, et al. Lentiviral-mediated miRNA against osteopontin suppresses tumor growth and metastasis of human hepatocellular carcinoma. Hepatology 2008;48:1834–42.
13. Wai PY, Kuo PC. Osteopontin: regulation in tumor metastasis. Cancer Metastasis Rev 2008;27:103–18.
14. Crawford HC, Matrisian LM, Liaw L. Distinct roles of osteopontin in host defense activity and tumor survival during squamous cell carcinoma progression *in vivo*. Cancer Res 1998;58:5206–15.
15. Hsieh YH, Juliana MM, Hicks PH, Feng G, Elmets C, Liaw L, et al. Papilloma development is delayed in osteopontin-null mice: implicating an antiapoptosis role for osteopontin. Cancer Res 2006;66:7119–27.
16. Ohyama Y, Nemoto H, Rittling S, Tsuji K, Amagasa T, Denhardt DT, et al. Osteopontin-deficiency suppresses growth of B16 melanoma cells implanted in bone and osteoclastogenesis in co-cultures. J Bone Miner Res 2004;19:1706–11.
17. Aslakson CJ, Miller FR. Selective events in the metastatic process defined by analysis of the sequential dissemination of subpopulations of a mouse mammary tumor. Cancer Res 1992;52:1399–405.
18. Shibata MA, Morimoto J, Otsuki Y. Suppression of murine mammary carcinoma growth and metastasis by HSVtk/GCV gene therapy using *in vivo* electroporation. Cancer Gene Ther 2002;9:16–27.
19. Shibata MA, Ito Y, Morimoto J, Otsuki Y. Lovastatin inhibits tumor growth and lung metastasis in mouse mammary carcinoma model: a p53-independent mitochondrial-mediated apoptotic mechanism. Carcinogenesis 2004;25:1887–98.
20. Sangaletti S, Di Carlo E, Gariboldi S, Miotti S, Cappetti B, Parenza M, et al. Macrophage-derived SPARC bridges tumor cell–extracellular matrix interactions toward metastasis. Cancer Res 2008;68:9050–9.
21. Song G, Cai QF, Mao YB, Ming YL, Bao SD, Ouyang GL. Osteopontin promotes ovarian cancer progression and cell survival and increases HIF-1alpha expression through the PI3-K/Akt pathway. Cancer Sci 2008;99:1901–7.
22. Ashkar S, Weber GF, Panoutsakopoulou V, Sanchirico ME, Jansson M, Zawaideh S, et al. Eta-1 (osteopontin): an early component of type-1 (cell-mediated) immunity. Science 2000;287:860–4.
23. Pollard JW. Tumour-educated macrophages promote tumour progression and metastasis. Nat Rev Cancer 2004;4:71–8.
24. Yang L, Huang J, Ren X, Gorska AE, Chytil A, Aakre M, et al. Abrogation of TGF beta signaling in mammary carcinomas recruits Gr-1^{+}CD11b^{+} myeloid cells that promote metastasis. Cancer Cell 2008;13:23–35.
25. Bunt SK, Yang L, Sinha P, Clements VK, Leips J, Ostrand-Rosenberg S. Reduced inflammation in the tumor microenvironment delays the accumulation of myeloid-derived suppressor cells and limits tumor progression. Cancer Res 2007;67:10019–26.
26. Simpson KD, Templeton DJ, Cross JV. Macrophage migration inhibitory factor promotes tumor growth and metastasis by inducing myeloid-derived suppressor cells in the tumor microenvironment. J Immunol 2012;189:5533–40.
27. DeNardo DG, Barreto JB, Andreu P, Vasquez L, Tawfik D, Kolhatkar N, et al. CD4(+) T cells regulate pulmonary metastasis of mammary carcinomas by enhancing protumor properties of macrophages. Cancer Cell 2009;16:91–102.

Published OnlineFirst July 17, 2014; DOI: 10.1158/0008-5472.CAN-13-3334

28. Tan W, Zhang W, Strasner A, Grivennikov S, Cheng JQ, Hoffman RM, et al. Tumour-infiltrating regulatory T cells stimulate mammary cancer metastasis through RANKL–RANK signalling. Nature 2011;470:548–53.
29. Dolcetti L, Peranzoni E, Ugel S, Marigo I, Fernandez Gomez A, Mesa C, et al. Hierarchy of immunosuppressive strength among myeloid-derived suppressor cell subsets is determined by GM-CSF. Eur J Immunol 2010;40:22–35.
30. Gabrilovich DI, Ostrand-Rosenberg S, Bronte V. Coordinated regulation of myeloid cells by tumours. Nat Rev Immunol 2012;12:253–68.
31. Shinohara ML, Kim HJ, Kim JH, Garcia VA, Cantor H. Alternative translation of osteopontin generates intracellular and secreted isoforms that mediate distinct biological activities in dendritic cells. Proc Natl Acad Sci U S A 2008;105:7235–9.
32. Hanahan D, Coussens LM. Accessories to the crime: functions of cells recruited to the tumor microenvironment. Cancer Cell 2012;21:309–22.
33. Lu P, Weaver VM, Werb Z. The extracellular matrix: a dynamic niche in cancer progression. J Cell Biol 2012;196:395–406.
34. Shevde LA, Samant RS, Paik JC, Metge BJ, Chambers AF, Casey G, et al. Osteopontin knockdown suppresses tumorigenicity of human metastatic breast carcinoma, MDA-MB-435. Clin Exp Metastasis 2006;23:123–33.
35. Chakraborty G, Jain S, Patil TV, Kundu GC. Down-regulation of osteopontin attenuates breast tumour progression *in vivo*. J Cell Mol Med 2008;12:2305–18.
36. Behera R, Kumar V, Lohite K, Karnik S, Kundu GC. Activation of JAK2/STAT3 signaling by osteopontin promotes tumor growth in human breast cancer cells. Carcinogenesis 2010;31:192–200.
37. Dai J, Li B, Shi J, Peng L, Zhang D, Qian W, et al. A humanized anti-osteopontin antibody inhibits breast cancer growth and metastasis *in vivo*. Cancer Immunol Immunother 2010;59:355–66.
38. Yang L, Wei L, Zhao W, Wang X, Zheng G, Zheng M, et al. Down-regulation of osteopontin expression by RNA interference affects cell proliferation and chemotherapy sensitivity of breast cancer MDA-MB-231 cells. Mol Med Rep 2012;5:373–6.
39. Sinha P, Clements VK, Ostrand-Rosenberg S. Reduction of myeloid-derived suppressor cells and induction of M1 macrophages facilitate the rejection of established metastatic disease. J Immunol 2005;174:636–45.
40. Bunt SK, Sinha P, Clements VK, Leips J, Ostrand-Rosenberg S. Inflammation induces myeloid-derived suppressor cells that facilitate tumor progression. J Immunol 2006;176:284–90.
41. Shibata MA, Yoshidome K, Shibata E, Jorcyk CL, Green JE. Suppression of mammary carcinoma growth *in vitro* and *in vivo* by inducible expression of the Cdk inhibitor p21. Cancer Gene Ther 2001;8:23–35.
42. Tripodo C, Sangaletti S, Guarnotta C, Piccaluga PP, Cacciatore M, Giuliano M, et al. Stromal SPARC contributes to the detrimental fibrotic changes associated with myeloproliferation whereas its deficiency favors myeloid cell expansion. Blood 2012;120:3541–54.